Facile Techniques to Synthesize Reduced Graphene Oxide for Removing Tetracycline From Water: Kinetics and Thermodynamics Studies

Trinh Tran Dinh (trinhtd@vnu.edu.vn)
University of Science https://orcid.org/0000-0001-9936-1823
Thi-My-Trinh Ha
University of Science
Thi-An-Hang Nguyen
Viet Nam Japan University
Viet-Cuong Dang
University of Science
Van-Duong Dao
Phenikaa University

Research Article

Keywords: Tetracycline, adsorption, influencing parameters, thermodynamics, kinetics, regeneration

Posted Date: October 1st, 2021

DOI: https://doi.org/10.21203/rs.3.rs-950512/v1

Facile techniques to synthesize reduced graphene oxide for removing tetracycline from water: kinetics and thermodynamics studies

Dinh-Trinh Tran[1,*], Thi-My-Trinh Ha[1], Thi-An-Hang Nguyen[2], Viet-Cuong Dang[1], Van-Duong Dao[3]

[1] VNU Key Lab. of Advanced Materials for Green Growth, University of Science, Vietnam National University, Hanoi, No. 19 Le Thanh Tong St., Hoan Kiem Dist., Hanoi, 11021, Vietnam

[2] Viet Nam Japan University (VNU-VJU), Vietnam National University, Hanoi, Luu Huu Phuoc St., Nam Tu Liem Dist., Hanoi, 101000, Vietnam

[3]Faculty of Biotechnology, Chemistry and Environmental Engineering, Phenikaa University, Hanoi, 10000, Vietnam

[*]Corresponding author: Dinh-Trinh Tran

Email: trinhtd@vnu.edu.vn

Abstract

In this study, reduced graphene oxide (rGO) was successfully produced from graphite precursor by chemical oxidation and exfoliation processes which were followed by a reduction process in mild conditions. rGO was then applied in the adsorption of tetracycline (TC) in water. SEM/EDX, XRD, FT-IR, BET, pH_{pzc} were conducted to characterize the synthesized materials. The adsorption efficiency of TC from water was evaluated by changes in several factors such as contact time, temperature, pH of the solution, adsorbent load, and tetracycline concentration. Furthermore, adsorption kinetics, thermodynamics, and isotherms were also investigated. As the result, the adsorption process of TC onto rGO was spontaneous, endothermic, and governed by

both physisorption and chemisorption. The maximum uptake calculated from Langmuir isotherm model was 58.03 mg/g. rGO material could be regenerated by using methanol and diluted NaOH solutions. The findings in this work provides a complete data on the TC adsorption process onto rGO and the process of recovery and reuse of rGO.

Keywords: Tetracycline, adsorption, influencing parameters, thermodynamics, kinetics, regeneration.

Introduction

Since their discovery in 1928, antibiotics have played a very important role in human health protection and the livestock industry. They have been extensively and effectively used in human and veterinary medicines and their benefits have also been recognized in agriculture, aquaculture, bee-keeping, and livestock as growth promoters [1]. It is estimated that millions of people have been saved from diseases (smallpox, cholera, typhoid fever, syphilis, etc.) thanks to antibiotics.

Intensive use of antimicrobials in livestock is a global trend. Van Boeckel et al. [2] estimated that global consumption of antimicrobials in animal food production was 63,151 (±1,560) tons in 2010, then doubled in 2013 (~131.109 tons) and expected to reach 200,235 tons by 2030 [2, 3]. The increasing usage of antibiotics raised a concern about the effect of their residue to the environment and human health. Beek et al. [4] collected data from more than 1000 publications about pharmaceutical concentrations and found that pharmaceuticals in the environment were truly a topic of global concern when it detected in 71 countries all around the world. The antibiotic – containing wastewater is the main factor contributing to the promotion of bacterial resistance genes, antibiotic resistant bacteria and some allergic reactions in human and

48 animals [5, 6]. Antibiotic-resistant infections also contribute to the financial burden on healthcare
49 systems.

50 Tetracycline (TC) antibiotics are one of the primarily antibiotics groups used for veterinary
51 purposes, for human therapy and in agriculture sector as feed additive [7]. According to Chen et
52 al. [8] tetracyclines are ranked second in the production and usage of antibiotics worldwide and
53 are ranked first place in China. Tetracycline is high water solubility (0.041mg/L) and low volatility
54 (low log K_{OW}). Therefore, it likely is persistent in the aquatic environment. Tetracycline was
55 detected 0.151µg/L (median) and 0.977µg/L (maximum) in wastewater treatment plants [9] and
56 municipal wastewater treatment plants effluent samples [10].

57 Several techniques have been developed to efficiently and effectively remove TC residues
58 from water such as membrane filtration [11] adsorption [12], and advanced oxidation processes
59 [13-16]. Among these methods, adsorption was a simple treatment method; it was affordable, easy
60 to handle with simple equipment, and low cost. In addition, the adsorbent could be recycled and
61 able to reuse several times. There were various mechanisms that affect the accumulation of
62 adsorbates on the surface of adsorbent like $\pi - \pi$ interaction, electrostatic interaction, and pore-
63 filling mechanism [17, 18].

64 Graphene is a single layer of carbon with thickness as a carbon molecule, dense with sp^2
65 carbon molecules in honeycomb lattice [19]. Graphene oxide (GO) is oxidized graphene and has
66 the presence of oxygen-containing functional groups while reduced graphene oxide (rGO) is
67 obtained from the reduction of GO by removing oxygen-containing functional groups. There were
68 differences in functional groups or C:O ratio between GO and rGO [20, 21]. Although the presence
69 of oxygen-containing groups make GO able to be hydrophilic which is suitable for water treatment,
70 they usually weaken the π-electron activity linked to a high fraction of sp^3 C atoms, which is

important interaction in the adsorption process [20]. On the other hand, rGO had a large specific surface area and significantly fewer functional groups than GO [22, 23]. Therefore, rGO is a promising adsorbent for the treatment of different pollutants. Huízar-Félix et al. [24] reported about the removal of TC using magnetic rGO material, which was expected to increase electrostatic interaction between rGO with the TC and recoverability. rGO also showed a rather high adsorption capacity for TC/sulfamethazine mixture (277.76 mg/g) than each substance (219.10mg/g for TC and 174.42mg/g for sulfamethazine) [25]. However, there is a lack of research conducting a complete study on the effect of different parameters on the adsorption of TC by rGO, which provide fully information of the adsorption of TC by rGO.

This paper aims to synthesize rGO from graphite precursor by chemical reduction of GO using L-ascorbic acid and employ rGO material to study the TC adsorption process. The effect of cintact time, temperature, initial pH, adsorbent dosage, initial TC concentration, and stability and reusability of the material will be investigated. Furthermore, the adsorption isotherms, adsorption kinetics, adsorption thermodynamics will be reported.

2. Experimental

2.1. Chemicals

Tetracycline powder (95.3% purity) were purchased from LKT Laboratories, Inc (Japan). Tetracycline stock solutions (100mg/L) were prepared by dissolving TC powder in double distilled water and stored at 4°C. Graphite fine powder extra pure were obtained for Merck (Germany). Concentrated sulfuric acid (H_2SO_4), sodium nitrate ($NaNO_3$), potassium permanganate ($KMnO_4$), hydrogen peroxide (H_2O_2), hydrochloric acid (HCl), L-ascorbic acid ($C_6H_8O_6$), nitric acid (HNO_3),

and sodium hydroxide (NaOH) were purchased from Xilong Scientific Co., Ltd. (China). All of the reagents used were of analytical grade.

2.2. Preparation of reduced graphene oxide

GO was synthesized by using modified Hummer's methods [15, 16]. The oxidation of graphite was conducted with the mixture of $KMnO_4$, H_2SO_4, $NaNO_3$. The obtained product was washed several times with doubly distilled water and then dried at 50°C overnight.

rGO was synthesized by the chemical reduction method using L-ascorbic acid. 1 gram of L-ascorbic acid is dissolved in 100 ml of distilled water. After adding 0.1 g of GO, the mixture was ultrasonicated in 45 minutes, then heated to 90~95°C for 1 hour. After the reaction time, the black precipitate was filtered by a vacuum pump and further washed by 1 M HCl and doubly-distilled water until a neutral pH value was achieved. Finally, the solid product was dried in a vacuum oven at 60°C for 4 hours.

2.3. Characterization of rGO material

X-ray powder diffraction (XRD) patterns were analyzed by X-ray diffraction spectroscopy (Miniflex 600, Rigaku, Japan) using Cu Kα radiation source (λ = 1.5418 Å) operated at a scan rate of $0.03^o.s^{-1}$ within a 2θ range from 5^o–70^o. Surface morphology and elemental composition of the material were performed by JSM-IT100/JED-2300 Analysis station, JEOL. Fourier Transform Infrared Spectroscopy (FT-IR) were recorded on an IR spectrometer Jasco 4600 (Japan) with a resolution of 4 cm^{-1} in the range of 400-4000 cm^{-1} at room temperature. Surface areas of the synthesized materials were measured by the Brunauer-Emmett-Teller method performed by a NOVAtouch LX^4. The point of zero charges of the sample was examined by pH drifting method as presented in our previous work [16]. The calculation of crystalline particles from XRD data, the Debye - Scherrer equation was used as follows:

$$D = \frac{0.9.\lambda}{\beta.cos\theta} \quad \text{(Eq. 1)}$$

where λ is the X-ray wavelength of Cu–Kα radiation source (λ = 0.15418 nm), β (in radians) is the full width at half maximum (FWHM) intensity of the diffraction peak located at 2θ, and β *is* the Bragg angle.

2.4. Batch experiments

Batch experiments were performed as the following procedure: Firstly, 100 mL of 10 mg/L TC solution was prepared from 1000 mg/L TC stock solution then transferred to a conical flask. Subsequently, 10 mg of the rGO material was added to the solution. The mixture was shaken at 120 rpm. 2 mL of solution was sampled at an interval time of 1 hour, filtered to determine the remaining TC concentration in the solution by UV–Vis spectroscopy (model UH5300/Hitachi, Japan) at an optimal wavelength of 358 nm. To evaluate the impact of solution pH on the adsorption efficiency of rGO, the pH value of the examined solutions was adjusted within the range of 2 to 10 while other conditions were unchanged. The impact of adsorbent dose on the adsorption efficiency of rGO was examined by varying rGO concentrtion from 50 mg/L to 250 mg/L, and keeping other parameters unchanged. Similarly, the influence of initial TC concentrations on rGO adsorption efficiency was tested within the range of 5 mg/L to 80 mg/L. Finally, the impact of temperature was examined with three temperature 298 K, 308K, and 318K. It is noted that all the experiments were conducted in triplicate.

2.4.1. Adsorption isotherm models

The adsorption uptake for TC removal q_t (mg/g) at time t was calculated by the equation (1):

$$q_t = \frac{(C_0 - C_t).V}{m} \quad \text{(Eq. 2)}$$

where C_0 (mg/L) and C_t (mg/L) are the TC initial concentrations and at time t (min), respectively. V is the volume of TC solutions (L); m is rGO mass (g).

The Langmuir (Eq. 3) and Freundlich (Eq. 4) are the two most commonly used isotherm models for describing the adsorption of pollutants onto graphene-based adsorbents [26].

$$q_e = \frac{q_{max}.b.C_e}{(1+b.C_e)} \quad \text{(Eq. 3)}$$

$$q_e = K.(C_e)^n \quad \text{(Eq. 4)}$$

where q_{max} is the Langmuir maximum uptake (mg/g), C_e is the equilibrium solution sorbate concentration (mg/L), and n is the Freundlich linearity constant. b and K designate the Langmuir bonding term related to the interaction energies (L/mg) and the Freundlich affinity coefficient ($L^n.mg^{(1-n)}/g$), respectively.

The Langmuir model supposes homogeneous binding sites, with equivalent sorption energies, and no interaction between adsorbed pollutants whereas the Freundlich is an empirical model related to an exponential distribution of adsorption sites and energies. The parameters obtained from the Langmuir and Freundlich models reveal important information on the surface property and affinity of the adsorbent as well as the sorption mechanism. In this report, the experimental data is fitted with Langmuir and Freundlich isotherm models by using OriginLab software version 9.0, OriginLab Corporation).

2.4.2. Adsorption kinetics modeling

In this work, pseudo-first-order, pseudo-second-order, and intra-particle diffusion models were deployed to examine the adsorption kinetics. They can be written as the following where the pseudo-first-order, pseudo-second-order, and intra-particle diffusion models are presented in equations 5, 6, and 7, respectively.

$$\ln(q_e - q_t) = \ln q_e - K_1.t \quad \text{(Eq. 5)}$$

$$\frac{t}{q_t} = \frac{1}{K_2.q_e^2} + \frac{t}{q_e} \quad \text{(Eq. 6)}$$

$$q_t = K_3.t^{1/2} + C \quad \text{(Eq. 7)}$$

where q_e and q_t are the adsorption uptake of TC at equilibrium and at time t (min) while K_1 (1/min) is the adsorption rate constant, K_2 (g/mg.min) is the rate constant of the second-order model, K_3 (mg/g.min$^{1/2}$) is the rate constant of the intra-particle diffusion model, and C is the intercept.

These kinetics models were evaluated in terms of the normalized standard deviation $\triangle q$ (%), which is calculated as:

$$\Delta q(\%) = \frac{(q_{e,exp} - q_{e,cal})}{q_{e,exp}}.100 \quad \text{(Eq. 8)}$$

2.4.3. Adsorption thermodynamics modeling

Thermodynamic characteristics of TC adsorption processes onto rGO were evaluated by thermodynamic parameters which involved changes in Gibbs free energy (G), enthalpy (H), and entropy (S). These parameters can be expressed as follows:

$$\Delta G = -RTln(K_d) \quad \text{(Eq. 9)}$$

$$K_d = \frac{q_e}{C_e} \quad \text{(Eq. 10)}$$

$$\Delta G = \Delta H - T.\Delta S \quad \text{(Eq. 11)}$$

$$ln(K_d) = \frac{\Delta S}{R} - \frac{\Delta H}{RT} \quad \text{(Eq. 12)}$$

where R: the universal gas constant = 8.314 (J/mol K), T: the temperature (K), and K_d: the distribution coefficient for the adsorption of TC.

2.4.4. Regeneration of the adsorbent

The regeneration of adsorbent is an important factor to evaluate the application of the process in reality. In this work, three successive cycles of adsorption–desorption were conducted. rGO

adsorbent was first washed several times with methanol 99.6%, then shaken in 0.1 M NaOH solution for 12 hours. In the subsequent step, the adsorbent was washed with distilled water to reach pH7 (verification by a pH meter HI2210-02, Hanna Instruments) prior to using for the next adsorption experiment.

3. Results and discussion

3.1. Characterization of materials

The XRD patterns of rGO, GO, and graphite are presented in the Fig 1. It can be clearly seen that characteristic peaks of graphite at $2\theta = 26.6^{o}$ and 54^{o}. The peak at 26.6^{o} was shifted to 10.62^{o}, characterizing the presence of GO crystalline structure [17, 24, 15], indicated that the graphite was fully oxidized. The broaden peak for rGO at $2\theta = 24.6^{o}$ implied that the rGO structure was arranged randomly, resulting in the formation of a single or only a few layers of rGO. A weak intensity peak at $2\theta = 42.88^{o}$ might be attributed to the turbostratic structure of disordered carbon materials [16, 29, 30].

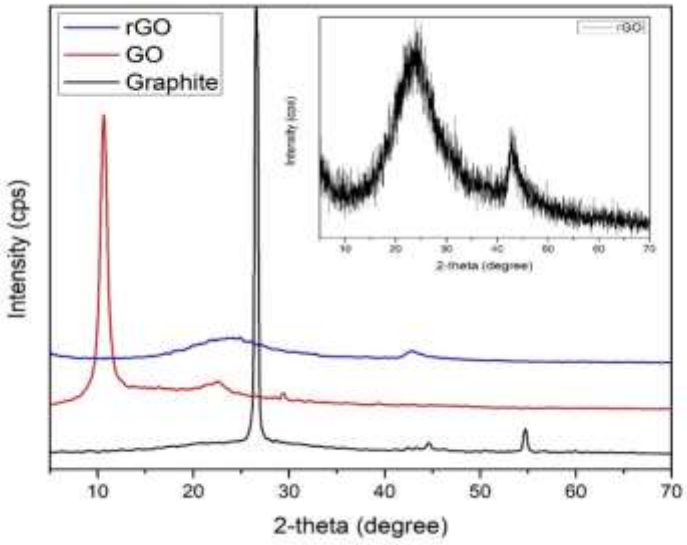

Fig. 1 XRD pattern of graphite, GO, and rGO materials.

The interlayer distance of GO was 8.33 Å, which was 2.5 times higher than the interlayer distance of graphite precursor (calculated from Eq.1). This phenomenon might be explained by the insertion of oxygen functional groups in the graphite plate after oxidation [27]. The interlayer distance of rGO was 3.59 Å, which was significantly decreased due to the elimination of various oxygen-containing functional groups after the chemical reduction [28].

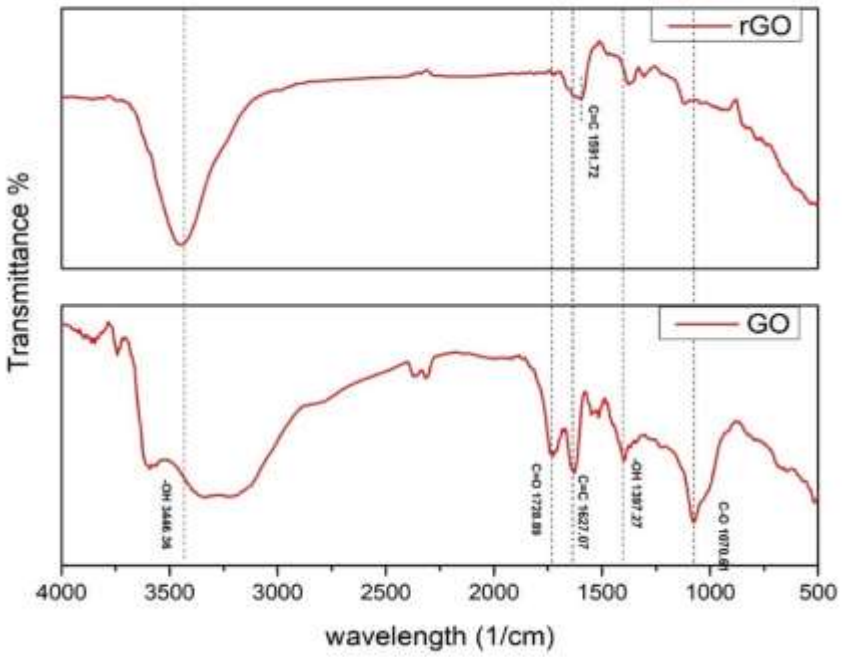

Fig. 2 FT – IR spectrum of GO and rGO materials.

Functional groups of GO and rGO were examined with the aid of the FT-IR method, and the corresponding spectrum of GO and rGO were shown in Fig. 2. The spectrum of GO shows several similarities with previous studies, consisted of an intense peak at 3446 cm^{-1} and other weak intensity peaks at 1728, 1627, and 1070 cm^{-1}, which might be associated with the vibration of O-H, C=O, C=C, and O-C-O, respectively [15, 16, 31]. It was noted that the rGO spectrum witnessed a diminish in the intensity of the peak at 1728 cm^{-1}, 1397 cm^{-1}, and 1070 cm^{-1}, which indicated the reduction of aldehyde (C=O) groups, tertiary C-OH groups, and alkoxy groups. The appearance

of an intense peak at 1591 cm^{-1} confirmed the restoration of the sp^2 carbon networks [32]. The obtained results suggested the reduction of oxygen-containing groups by L-Ascorbic acid. This observation was also confirmed by the EDX analysis presented in the subsequent section.

The images of graphite and rGO are described in Fig. 3a and 3b, respectively. It was shown that the graphite's structure was characterized by several layers stacked while rGO took a typical wrinkled morphology.

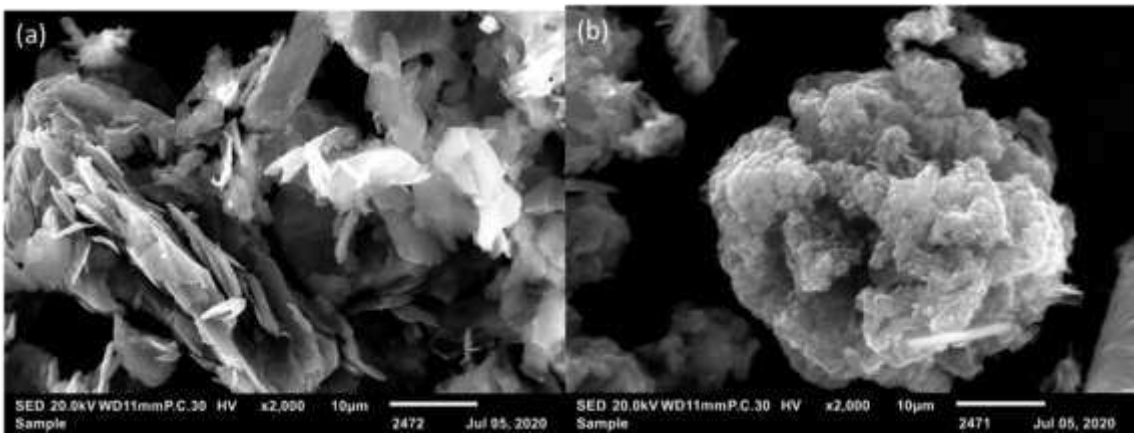

Fig. 3 SEM images of (a) graphite and (b) rGO materials.

The elemental composition of the material was examined by the EDX method. The C/O ratio in GO and rGO materials were respectively 1.07 and 7.10 (Table 1), implying that the removal of oxygen-containing functional groups led to the reduction of oxygen element in the rGO sheets. The obtained results in this work were comparable with previously reported results, which applied different reduction methods (Table 1). It is noted that the reduction of GO by L–ascorbic acid is milder and more acceptable than the use of $NaBH_4$ or hydrazine, which can result in the formation of toxic gases and/or damage to the product's structure [33].

Table 1. Elemental composition of materials in this study and previous studies.

Material	C/O atomic ratio	Reduction agent	References
Graphite	23.75		
GO	1.07	L-ascorbic acid	This study
rGO	7.10		
Graphite	17.87		
GO	2.65	L-ascorbic acid	[33]
rGO	2.89-5.15		
rGO	5.38	$NaBH_4$, $CaCl_2$ (catalyst)	[34]
GO	2.23	*Azotobacter chroococcum*	[8]
rGO	4.18		
rGO	6.87 – 6.97	$NaBH_4$	[35]
rGO	15.1	Hydrazine	[36]
rGO	2.73 – 3.64	Starch	[37]
rGO	7.75	Aluminum powder	[38]

The BET analyses are displayed in Fig. 4. The N_2 adsorption-desorption isotherm was characterized by type IV and the H3 hysteresis loop [15]. Type IV isotherm was associated with capillary condensation taking place in mesopores, while the H3 hysteresis loop exhibited the aggregates of micropores associated with plate-like particles giving rise to slit-shaped pores [15]. The pore-size distribution in rGO presented two typical peaks with a half pore width of ~3.2 nm and about 12 nm while most of the pores had a radius below 25 nm, suggesting that synthesized rGO was mesoporous material. The specific surface area of rGO was 341.2 m^2/g, significantly higher than that of graphite (7.78 m^2/g). The surface area of rGO was quite lower than the theoretical value (around 2,500 m^2/g) could be attributed to tight hydrogen bonding and the formation of aggregates from rGO sheets when the solvents were removed [39, 40].

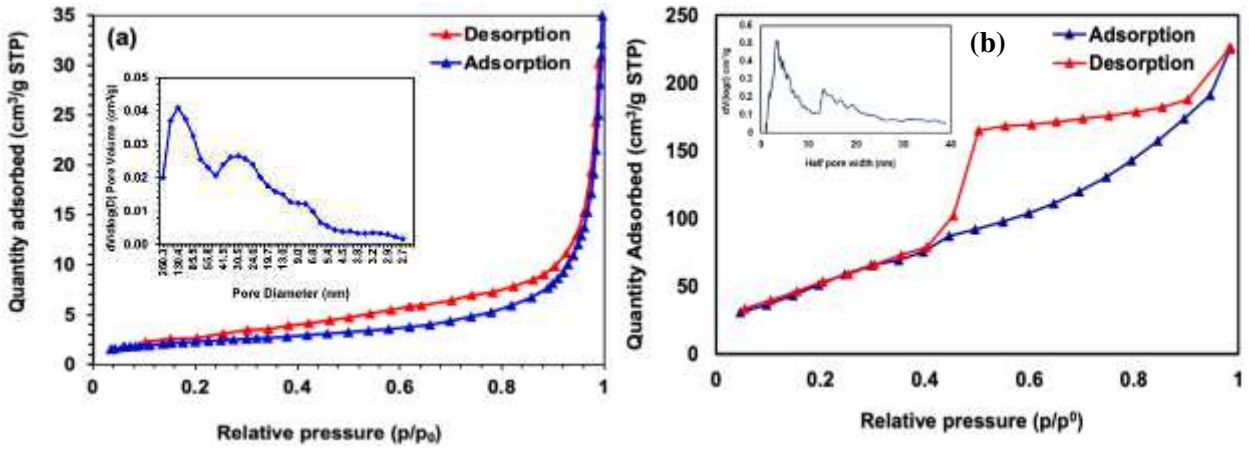

Fig. 4 Nitrogen adsorption – desorption isotherm and pore size distribution of (a) graphite and (b) rGO samples.

Point of zero charges (pH_{pzc}) is when the surface charge of the material equals zero. In this work, the pH_{pzc} of the rGO material was 5.2, implying that the rGO surface was positively charged in pH < 5.2 solutions while it was negatively charged pH>5.2 solutions.

3.2. TC adsorption processes onto rGO material

3.2.1. Effect of contact time and pH

The obtained results are shown in Fig. 5. It was clear that the adsorption uptake of rGO quickly increased during the first 6 hours, reached 46.45 mg/g, then remained relatively stable afterward, suggesting that the equilibrium time for the adsorption of TC by rGO was 6 hours (Fig. 5a). The initial pH of TC solutions was prepared in the range of 2–10 to study the impact of the pH value on the adsorption of TC onto rGO. When the initial pH value increased from 2 to 7, the adsorption capacity of rGO material augmented, reaching the maximum value of 30.92 (mg/g) at pH7 (Fig. 5b). This could be explained by the fact that when the pH < 4, the TC molecules were fully protonated [20] while rGO surfaces were positively charged as the pH_{pzc} of rGO = 5.2, which would inhibit the accumulation of TC on the surfaces of rGO due to the electrostatic repulsive

force. In the range of pH4 – pH7, the TC was in the form of zwitterion + − 0, the interaction between rGO and TC molecules was impacted by both electrostatic repulsion and attraction forces. As a result, the adsorption of TC molecules on rGO was controlled by the stronger one. In pH > 7.7 solutions, TC was in the form of monovalent anion, + − −, or a divalent anion, 0 − − [15, 41]. This explained a decline in adsorption capacity of rGO in the pH ≥ 8 solutions (Fig. 5b) due to the electrostatic repulsion between rGO surface negatively charged and TC anions.

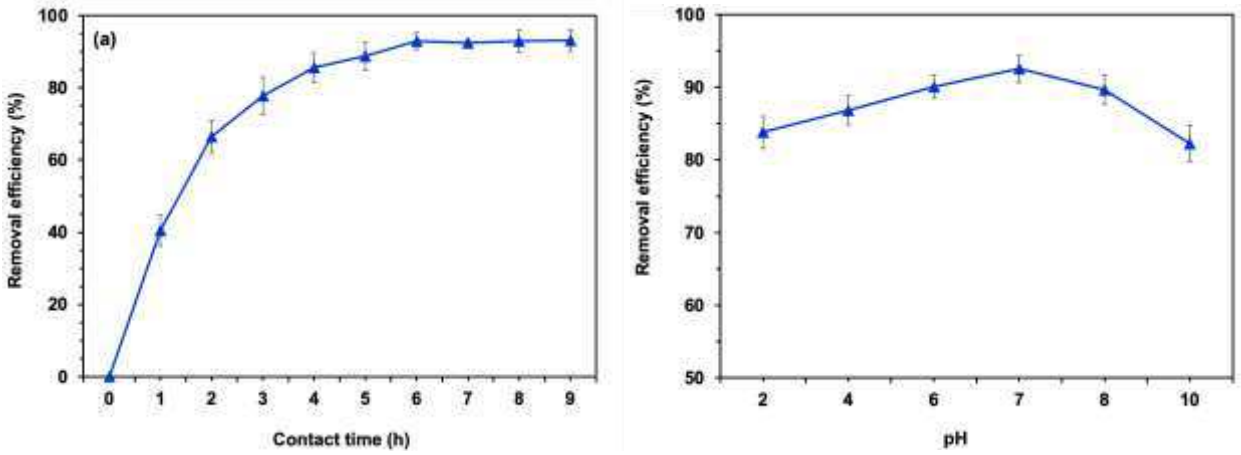

Fig. 5 Effect of (a) contact time and (b) pH on the removal eficiency of rGO (adsorption conditions: [TC] = 5 mg/L, pH=6.5, m_{rGO} = 10 mg, V = 100 mL).

In addition to electrostatic interactions between rGO and TC molecules, the competitive adsorption between H^+ and TC in acidic solutions and between OH^- and TC in basic medium, the π – π interactions between TC and the aromatic structure of rGO dramatically enhanced the adsorption energy of rGO and TC, leading to an improvement of adsorption capacity [20].

3.2.2. Effect of adsorbent dosage

The adsorbent dosage might affect the adsorption process because it supplies more available sites for TC molecules to be adsorbed. The results in Fig. 6a show that the adsorption capacity decrease in correlation with an increase in adsorbent load from 50 mg/L to 100 mg/L. The maximum uptake reached 46.29 mg/g, corresponding to the adsorbent load of 100 mg/L.

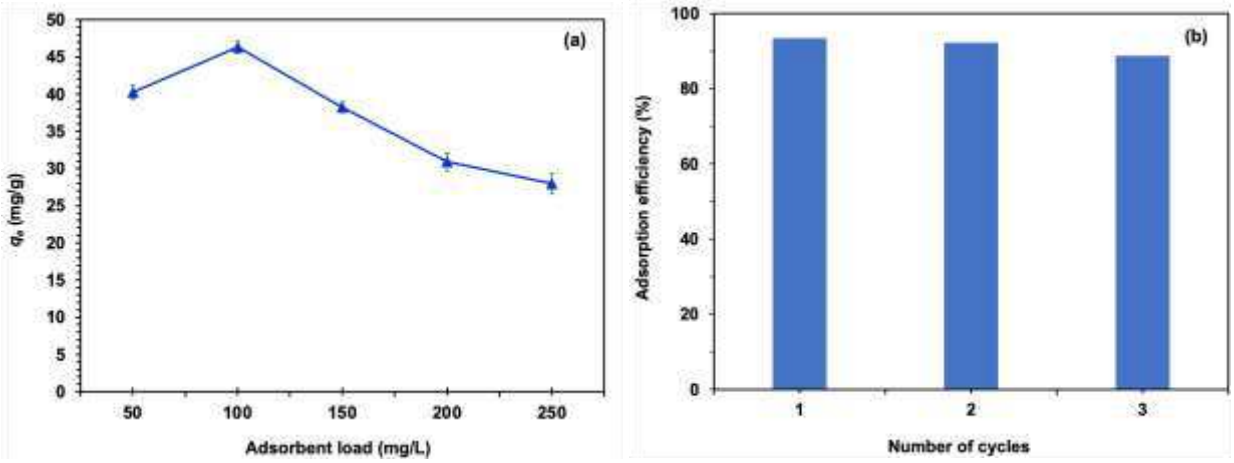

Fig. 6 (a) Effect of adsorbent dosage on TC removal by rGO, and (b) regeneration of rGO (adsorption conditions: [TC] = 5 mg/L, pH = 7.0, m_{rGO} = 10 mg, V = 100 mL).

When the adsorbent dose exceeded 100 mg/L, the adsorption capacity of rGO declined. These observations could be explained as 1) the total surface area became more important when rGO concentration increased, leading to better adsorption capacity. However, when the amount of the adsorbent exceeded 100 m/L, the aggregation of rGO sheets due to $\pi - \pi$ interactions occurred, which could contribute to a decline in total surface area. This results in a lower TC removal efficiency [42, 43].

3.2.3. Effect of initial concentration of TC: adsorption isotherms

The results in Fig 7a reveal that the higher the initial concentration of TC the better removal capacity. This observation could be attributed to (1) at lower TC concentrations, the mass transfer of TC molecules and the adsorbed fraction of ions became low, resulting in lower adsorption capacity; (2) when the TC concentration increased, the increase in mass the transfer of TC molecules led to a higher fraction of molecules occupied the available adsorption sites on the surface of materials, therefore increasing the adsorption yield. When the TC concentration achieved a limit value (around 60-70 mg/L), the number of unoccupied active sites might decrease, leading to a decline in adsorption capacity.

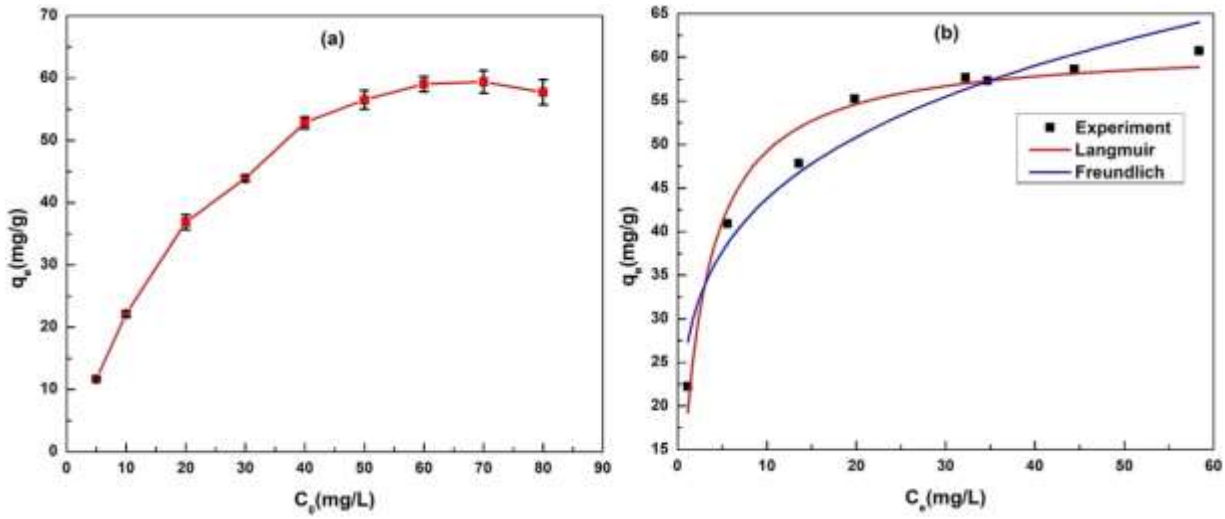

Fig. 7 (a) Effect of initial concentration of TC, and (b) adsorption isotherms (adsorption conditions: [TC] = 5 - 80 mg/L, pH = 7, m_{rGO} = 10 mg, V = 100 mL).

The experimental results were subsequently subjected to two adsorption isotherm models (Langmuir and Freundlich) for studying the adsorption isotherm. The obtained results in Fig. 7b depicted that the Langmuir model better described the adsorption of TC on rGO than the Freundlich model. This was supported by the slightly higher regression coefficient (R^2) by the Langmuir model than the one obtained by the Freundlich model (0.986 vs 0.942). This suggested that chemisorption with monolayer was more importantly governing the adsorption process. The maximum adsorption uptake calculated by Langmuir model achieved 58.03 mg/g. The obtained result in this work was higher than the one (13.27 mg/g) obtained from the adsorption of TC onto biochar [44] but lower than the result (313 mg/g) obtained from the adsorption of TC onto GO [17]. This could be explained by different functional groups (–OH, –C=O, –COOH, –O–) on the surface of GO, which might facilitate the accumulation of TC molecules by electrostatic attraction forces [24].

3.2.5. Effect of temperature

The effect of temperature was examined with 298K, 308K, and 318K. The adsorption capacities at the selected temperatures were compared at the equilibrium condition (6 hours). The experimental data revealed that the adsorption capacity was positively proportional to the temperature (Fig 8). For instance, the adsorption capacity of rGO for the removal of 80 mg/L TC solutions at 298K, 308K, 318K respectively reached 60.76, 107.33 and 137.41 mg/g while these values for 10 mg/L TC solutions were 40.95 mg/g; 43.13 mg/g; and 43.30 mg/g, respectively. This implied that the adsorption process would be endothermic in case it was associated with reversible adsorption.

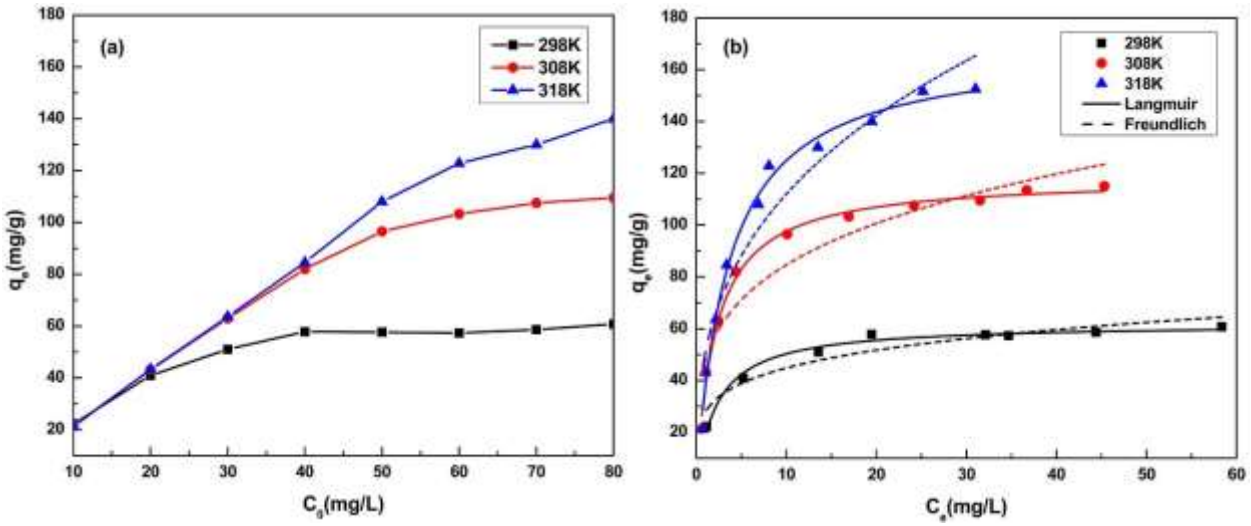

Fig. 8 (a) effect of temperature on the TC adsorption, (b) adsorption isotherms at different temperature (conditions: [TC] = 5 – 80 mg/L, pH = 7.0, m_{rGO} = 10 mg, V = 100 mL).

3.2.5. Adsorption kinetics

The results were better fitted with the pseudo-first-order model than the pseudo-second-order (regression coefficient (R^2) = 0,991 for the pseudo-second-order model compared with R^2= 0,998 for the pseudo-first-order model). In addition, the percentage deviations of q_e for the pseudo-first-order model was significantly lower than that obtained from the pseudo-second order model

329 (4.91% vs 34.2%), implying physisorption was predominant in the TC adsorption process (Table
330 2). The constant rate K estimated from the first-order model was 0.6356 h^{-1}. Table 2 also compares
331 the constant rate of different materials used for TC adsorption. It indicated that the adsorption rate
332 of rGO was higher than graphite and other materials such as pumice and biochar, but lower than
333 GO probably due to a number of oxygen-containing functional groups on the surface of GO, which
334 enhanced the adsorption of TC molecules by ion exchange and/or electrostatic attraction forces
335 [24].

336 Table 2. Comparison of kinetic parameters of different materials in the adsorption of TC.

Kinetic models		**Adsorbents**					
		rGO	**Graphite**	**Biochar**	**GO**	**rGO**	**Pumice**
Pseudo–1st order	q_e (experimental)	46.54	33.01	6.42	38.03	37.5	2.83
	q_e (mg/g)	48.71	31.51	3.27	-	-	2.93
	K (h^{-1})	0.6356	0.014	0.081	-	-	0.05
	R^2	0.998	0.99	0.877	-	-	0.99
	$\%\Delta q_e$	4.91	4.5	48.9	-	-	3.6
Pseudo–2nd order	q_e (mg/g)	62,50	-	7.01	35,03	44.23	2.99
	K ($g.mg^{-1}.h^{-1}$)	0.017	-	0.069	0.065	5.4	0.049
	R^2	0.991	-	0.99	0.99	0.991	0.98
	$\%\Delta q_e$	34.20	-	9.4	7.9	17.9	6.8
Intra -particle	K_d ($mg.g^{-1}.h^{-0.5}$)	0.0637	-	-	-	-	-
	C ($mg.g^{-1}$)	0.7591	-	-	-	-	-
	R^2	0,987	-	-	-	-	-
	References	This study	[45]	[44]	[17]	[24]	[46]

337

338

339 ***3.2.6. Adsorption thermodynamics and regeneration of adsorbent***

340 To assess energy exchange phenomenon of the TC sorption process, Gibbs free energy
341 (ΔG), enthalpy (ΔH), and entropy (ΔS) were estimated. ΔG values were negative at all temperature
342 (-7.79, -9.31, and -9.54 kJ/mol for 298, 308, and 318K) which confirmed the spontaneous nature
343 of the adsorption of TC onto rGO (Table 3).

344 Table 3. Thermodynamic parameters of TC adsorption process onto rGO.

Temperature (K)	**ΔG (kJ/mol)**	**ΔH (kJ/mol)**	**ΔS (kJ·mol^{-1}·K^{-1})**
298	-7.79		
308	-9.31	17.97	0.087
318	-9.54		

345

346 In general, the adsorption enthalpy in the range of 2 to 20 kJ/mol characterizes physical
347 adsorption. The positive value of ΔH (17.97 kJ/mol) confirmed that the adsorption process was
348 endothermic and physisorption (Table 3). It was noted that the results of adsorption isotherm
349 revealed that chemisorption with monolayer was more important process while the results on
350 adsorption thermodynamics and kinetics indidated physisorption played a more important role than
351 chemisorption; therefore, it could be concluded that the TC adsorption onto rGO was of both
352 physisorption and chemisorption. The positive value of ΔS (87 J.mol^{-1}.K^{-1}) reflected an increase
353 in the disorder and randomness at rGO-solution interfaces during the sorption of TC.

354 It is noted that the successive desorption–adsorption trial was repeated three times in which
355 adsorption test was performed at optimal conditions (10 mg rGO, 5 mg/L MB solution (pH=7),
356 and a contact time of 6 hours). The adsorption efficiency remained very high (> 89%) after three

cycles for TC adsorption (Fig 6b). This suggests that methanol and 0.1 M NaOH solutions could be deployed to regenerate rGO for further adsortion process.

Conclusions

The reduced graphene oxide was successfully synthesized using chemical reduction process with the aid of L – ascorbic acid as the reducing agent. Effects of different parameters on the adsorption of TC onto rGO material such as contact time, temperature, pH of the solution, adsorbent dosage, and TC initial concentration were studied. The optimal conditions for the adsorption of TC onto rGO were 6 hours, pH=7, adsorbent load = 100 mg/L, TC initial concentration = 60 mg/L. The TC adsorption process was better described by the pseudo-first-order model and the Langmuir adsorption isotherm model. The maximum uptake calculated by Langmuir model was 58.03 mg/g. The TC adsorption process was spontaneous, endothermic. Both chemisorption and physisorption mechanisms occurred during the TC adsorption process. The recovery and reuse of rGO could be performed by using methanol and diluted NaOH solutions, with a decrease of about 6% in adsorption efficiency after 3 cycles. This research revealed that the rGO was a promising material for the removal of TC from solutions.

Data availability

All data generated or analyzed during this study are included in this published article.

Conflicts of Interest Declaration

The authors declare that they have no known competing financial interests or personal relationships that could have appeared to influence the work reported in this paper.

References

1. R. Gothwal, T. Shasidhar, Clean (Weinh) 43, 479–489 (2015). https://doi.org/10.1002/clen.201300989.
2. T.P. van Boeckel, C. Brower, M. Gilber, B.T. Grenfell, S.A. Levin, T.P. Robinson, Proc. Natl. Acad. Sci. U.S.A 112, 5649–5654 (2015). https://doi.org/10.1073/pnas.1503141112.
3. T.P. van Boeckel, E.E. Glennon, D. Chen, M. Gilbert, T.P. Robinso, B.T. Grenfel, S.A. Levin, S. Bonhoeffer, R. Laxminarayan, Science. 357, 1350–1352 (2017). https://doi.org/10.1126/science.aao1495.
4. T. Beek, F.A. Weber, A. Bergmann, S. Hickmann, I. Ebert, A. Hein, A. Kuster, Environ. Toxicol. Chem. 35, 823–835 (2016). https://doi.org/10.1002/etc.3339.
5. M. Xua, J. Deng, A. Cai, X. Ma, J. Li, Q. Li, X. Li, Chem. Eng. J. 384, 123320 (2020). https://doi.org/10.1016/j.cej.2019.123320.
6. A. Cai, J. Deng, M. Xu, T. Zhu, S. Zhou, J. Li, G. Wang, X. Li, Chem. Eng. J. 395, 125090 (2020). https://doi.org/10.1016/j.cej.2020.125090.
7. B. Daghrir, P. Drogui, Environ. Chem. Lett. 11 209–227 (2013). https://doi.org/10.1007/s10311-013-0404-8.
8. Y. Chen, Y. Niu, T. Tian, J. Zhang, Y. Wang, Y. Li, L.C. Qin, Chem. Phys. Lett. 677, 143–147 (2017). https://doi.org/10.1016/j.cplett.2017.04.002.
9. X.S. Miao, F. Bishay, M. Chen, C.D. Metcalfe, Environ. Sci. Technol. 38 3533–3541 (2004). https://doi.org/10.1021/es030653q.
10. A. Javid, A. Mesdaghinia, S. Nesseri, A.M. Mahvi, M. Alimohammadi, H. Gharibi, J. Environ. Health Sci. Eng. 14, 4 (2016). https://doi.org/10.1186/s40201-016-0245-z.

11. Oh S-H, Jeong S, Kim I. S, Shon H. K, Jang A, J. Environ. Manage. 247, 385–393 (2019). https://doi.org/10.1016/j.jenvman.2019.06.070.
12. Y. Li, X. Lin, C. Zhang, Q. Zhuang, W. Dong, Colloids Surf. A Physicochem. Eng. Asp. 628, 127263 (2021). https://doi.org/10.1016/j.colsurfa.2021.127263
13. M.S.A. Hussien, J. Inorg. Organomet. Polym. 31, 945–959 (2021). https://doi.org/10.1007/s10904-020-01831-z
14. Y. Duan, Y. Cao, X. Shang, D. Jia & C. Li, J. Inorg. Organomet. Polym. 31, 2140–2149 (2021). https://doi.org/10.1007/s10904-021-01923-4
15. D.T Tran, V.N Nguyen, Mater. Res. Express 7, 075501 (2020). https://doi.org/10.1088/2053-1591/ab9e47
16. V.C. Dang, D.T. Tran, A.T. Phan, N.K. Pham, V.N. Nguyen, J. Phys. Chem. Solids 153, 110005 (2021). https://doi.org/10.1016/j.jpcs.2021.110005
17. Y. Gao, Y. Li, L. Zhang, H. Huang, J. Hu, S.M. Shah, X. Su, J. Colloid Interface Sci. 368, 540–546 (2012). https://doi.org/10.1016/j.jcis.2011.11.015.
18. N. Ninwiwek, P. Hongsawat, P. Punyapalakul, P. Prarat, Colloids Surf. A Physicochem. Eng. Asp. 580, 123716 (2019). https://doi.org/10.1016/j.colsurfa.2019.123716
19. R. Seki, H. Takamatsu, Y. Suzuki, Y. Oya, T. Ohba, Colloids Surf. A Physicochem. Eng. Asp. 628, 127393 (2021). https://doi.org/10.1016/j.colsurfa.2021.127393
20. K. Haubner, J. Murawski, P. Olk, L.M. Eng, C. Ziegler, B. Adolphi, E. Jaehne, Chemphyschem 11, 2131–2139 (2010). https://doi.org/10.1002/cphc.201000132.
21. Z. Liu, Z. Diao, Y. Yuan, H. Jia, L. Wang, W. Fei, Colloids Surf. A Physicochem. Eng. Asp. 620, 126573 (2021). https://doi.org/10.1016/j.colsurfa.2021.126573

22. Y. Ai, Y. Liu, Y. Huo, C. Zhao, L. Sun, B. Han, X. Cao, X. Wang, Environ. Sci. Nano 6, 3336–3348 (2019). https://doi.org/10.1039/C9EN00866G

23. P.V. Nidheesh, Environ. Sci. Pollut. Res. 24, 27047–27069 (2017). https://doi.org/10.1007/s11356-017-0481-5

24. A.M. Huízar–Félix, C. Aguilar–Flores, A.M. Cruz, J.M. Barandiarán, S. Sepúlveda–Guzmán, R. Cruz–Silva, Nanomaterials 9, 313 (2019). https://doi.org/10.3390/nano9030313.

25. W. Song, T. Yang, X. Wang, Y. Sun, Y. Ai, G. Sheng, T. Hayat, X. Wang, Environ. Sci. Nano 3, 1318–1326 (2016). https://doi.org/10.1039/C6EN00306K.

26. M. Aleksandrzak, D. Moszyński, E. Mijowska, J. Colloid Interface Sci. 496, 188–200 (2017). https://doi.org/10.1016/j.jcis.2017.02.031

27. J. Dai, X. Meng, Y. Zhang, Y. Huang, Bioresour. Technol. 311, 123455 (2020). https://doi.org/10.1016/j.biortech.2020.123455.

28. Z.J. Fan, W. Kai, J. Yan, T. Wei, L.J. Zhi, J. Feng, Y. Ren, L.P. Song, F. Wei, ACS Nano 5, 191–198 (2011). https://doi.org/10.1021/nn102339t.

29. J. Yan, Z. Fan, T. Wei, W. Qian, M. Zhang, F. Wei, Carbon 48, 3825–3833 (2010). https://doi.org/10.1016/j.carbon.2010.06.047.

30. H.M.A. Hassan, V. Abdelsayed, A.E.R.S. Khder, K.M.A. Zeid, J. Terner, M.S. El–Shall, S.I. Al–Resayes, A.A. El–Azhary, J. Mater. Chem. 19, 3832–3837 (2009). https://doi.org/10.1039/B906253J.

31. V.N. Nguyen, D.T. Tran, M.T. Nguyen, T.T.T. Le, M.N. Ha, M.V. Nguyen, T.D. Pham, Res. Chem. Intermed. 44, 3081–3095 (2018). https://doi.org/10.1007/s11164-018-3294-3

446 32. F.T. Johra, W.G. Jung, Appl. Surf. Sci. 357, 1911–1914 (2015).
447 https://doi.org/10.1016/j.apsusc.2015.09.128.
448 33. C. Xu, X. Shi, A. Ji, L. Shi, C. Zhou, Y. Cui, PLoS ONE 10, 0144842 (2015).
449 https://doi.org/10.1371/journal.pone.0144842.
450 34. Z. Yang, Q. Zheng, H. Qiu, J. Li, J. Yang, New Carbon Mater. 30, 41–47 (2015).
451 https://doi.org/10.1016/S1872-5805(15)60174-3.
452 35. L.G. Guex, B. Sacchi, K.F. Peuvot, R.L. Andersson, A.M. Pourrahimi, V. Strom, S. Farris,
453 R.T. Olsson, Nanoscale 9, 9562–9571 (2017). https://doi.org/10.1039/C7NR02943H
454 36. P.G. Ren, D.X. Yan, X. Ji, T. Chen, Z.M. Li, Nanotechnology 22, 055705 (2010).
455 http://dx.doi.org/10.1088/0957-4484/22/5/055705.
456 37. K.B. Narayanan, H.D. Kim, S.S. Han, Colloids Surf. B 185, 110579 (2020).
457 https://doi.org/10.1016/j.colsurfb.2019.110579.
458 38. Z. Fan, K. Wang, T. Wei, J. Yan, L. Song, B. Shao, Carbonn 48, 1686–1689 (2010).
459 https://doi.org/10.1016/j.carbon.2009.12.063.
460 39. P. Montes–Navajas, N.G. Asenjo, R. Santamaría, R. Menéndez, A. Corma, H. García,
461 Langmuir 29, 13443–13448 (2013). https://doi.org/10.1021/la4029904
462 40. H. Moussa, E. Girot, K. Mozet, H. Alem, G. Medjahdi, R. Schneider, Applied Catalysis
463 B: Environmental 185, 11–21 (2016). https://doi.org/10.1016/j.apcatb.2015.12.007.
464 41. A. Amat, S. Fantacci, F.D. Angelis, B. Carlotti, F. Elisei, Chem. Acc. 131, 1218 (2012).
465 https://doi.org/10.1007/s00214-012-1218-7.
466 42. K.S. Padmavathy, G. Madhu, P.V. Haseena, Procedia Technol. 24, 585–594 (2016).
467 https://doi.org/10.1016/j.protcy.2016.05.127.
468 43. P. Wang, J. Environ. Sci. 56, 202–213 (2017). https://doi.org/10.1016/j.jes.2016.04.032.

469 44. H. Wang, C. Fang, Q. Wang, Y. Chu, Y. Song, Y. Chen, X. Xue, RCS Adv. 8, 16260–
470 16268 (2018). https://doi.org/10.1039/C8RA01454J.
471 45. M.D. Vedenyapina, D.A. Borisova, A.K. Rakisev, A.A. Vedenyapin, Solid Fuel Chem.
472 48, 323–327 (2014). https://doi.org/10.3103/S0361521914050139.
473 46. J. Lu, K. Xu, W. Li, D. Hao, L. Qiao, Water Qual. Res. J. Canada 53, 143–155 (2018).
474 https://doi.org/10.2166/wqrj.2018.012.